International Journal of Mathematical, Engineering and Management Sciences
Vol. 7, No. 5, 749-763, 2022
https://doi.org/10.33889/IJMEMS.2022.7.5.049

Numerically Detection Fluid Characteristic Effects in Porous Media for Plastic Manufacturing Process Reconstruction

Muttaqin Rahmat Pangaribawa
Department of Mechanical Engineering,
Universitas Muhammadiyah Surakarta, Surakarta, Indonesia.
E-mail*:* muttaqin.r.pangaribawa@ums.ac.id

Sunardi Wiyono
Department of Mechanical Engineering,
Universitas Muhammadiyah Surakarta, Surakarta, Indonesia.
E-mail: sunardi_wiyono@ums.ac.id

Sarjito
Department of Mechanical Engineering,
Universitas Muhammadiyah Surakarta, Surakarta, Indonesia.
Corresponding author: sarjito@ums.ac.id

Niko Aji Sutopo
Department of Mechanical Engineering,
Universitas Muhammadiyah Surakarta, Surakarta, Indonesia.
E-mail: d200170220@student.ums.ac.id

Fiki Amirul Khusaini
Department of Mechanical Engineering,
Universitas Muhammadiyah Surakarta, Surakarta, Indonesia.
E-mail: d200190121@student.ums.ac.id

(Received on March 14, 2022; Accepted on August 08, 2022)

Abstract
Research work aimed to prove the cooling effectiveness and efficiency of heating numerically. It was carried out by reconstructing the mold to reduce condensation while keeping the production cycle time. The simulation was done using CFD Fluent, Finite Volume Method (FVM) with a solution method of pressure-velocity, SIMPLE coupling, and second-order upwind discretization scheme. The model's boundary condition represents plastic packaging's production process. The simulation was done to optimize performance during production. Reconstruction and simulation were undertaken. The initial investigation was to produce data for cooling time versus the whole production time. The research result indicated that the average cooling time was 3/5 of the total production time. There were 15.5706 of 26.4206 sec and 15.641 of 26.491 sec, respectively. Further investigation was focused on investigating heat absorption and transfer through cells in the matrix. The porous effect showed temperature gradient reduction between cooled and cooler temperatures by simulation in color. The phenomenon predicted that the R_a contributed to the rate of temperature decrease revealed. There is also an apparent increase in temperature interfaces is evidence. The porous media application with The Rayleigh Number $\geq 10^5$ retained the potential cooling effectivity and heating efficiency. By simulation, a series of discussions of the result of research, the potential may apply in the plastic mold to reconstruct the space and its methods using filling-porous. It is relevant because the heating ability in the phase change of fluid that creates particular characteristics has the potential to make effective cooling.

Keywords- Condensation, Detection, Fluid and mass transfer, Porous, Cooling.

1. Introduction

A refrigeration system to reduce the cooling time may be debated in the case of plastic production using a refrigeration system or reheating. In the plastic manufacturing process, the issue appeared when starting the machine again, so condensate appeared. Trial production requires many shots of products rejected and takes a long time for mold conditioning. Even refrigeration analysis was needed to release condensate besides reheating mold because a cooling system with the cooling device outside the mold section was ineffective. It must be cautious when using a 20 °C because lower temperatures cause more condensate.

The research statement about cooling from the inner mold to very slowly chill products stimulated cooling reconstruction in manufacturing (Leonard & Ryder, 1978). It was hard to control the cooling of the part, and even many features were too cool (Dale, 1984). In addition, there was research about cooling devices using the pump to cool the mold (Davis, 1993). In this situation, the cooling process was working from the outer part of the mold by using pump devices. At temperatures 5-20 °C, a lower cooling temperature could create cooling efficiency. However, condensate caused a defect in the next production cycle (Brdlík, 2017). Some devices have applied the reconstruction, such as rocket nozzle, water cooling, firefighter suits, and turbine blades. In this case, the research study about the potential of fluid movement increasing The Nusselt Number in a porous and the thermal conductivity was crucial (Ould-Amer et al., 1998). Numerically, a potential method to reconstruct the mold using porous calculated (Pangaribawa & Fauzun, 2019). The research mentioned a potential effect of air in the cooling system numerically with its experimental characteristics. Porosity should impact mass transfer (Wang & Lei, 2020). The consideration was the mathematics review about flowing fluid in a thin porous medium (Suárez-Grau, 2021). Nowadays, plastic mold is developed by flowing low-density cooler. It applied forced water cooling, which streamed into the inner part of the mold by manufacturing a conformal channel to wash and control the temperature (Kurtulus et al., 2021). However, it created manufacturing problems and debates about uniformity and the process's naturality. In addition, as mentioned by (Julianto et al., 2019), uncontrolled heating releases affect temperature changes and stress characteristics. In the case of product quality, research in the past found that heat can fracture the glass under heat radiation. As a solution, cells in a metal mold can increase the thermal conductivity by escalating the Nusselt Number.

Mold cooling using porous become the solution for adequate cooling. It depends on the consideration that a higher cooling temperature influences the fewer quantity of product. On the other hand, lower cooling temperature creates product defects. The research takes into account the holding capacity in the mold. The optimal design, called matrix with cells, symbolized V_s. The volume of a metal cavity or cell as $V_p = V\text{-}V_s$. So, the porosity is $P = V_f/V$. From this literation, characteristic fluid in a cell needs to study further.

As a principle, the temperature was the main factor in forming (Benrabah et al., 2013), there was the rate of crystallinity of the polymer (Brdlík, 2017), and the basis of the principle to resolve was liquid-gas phase change in increasing heat transfer (Ehlers & Häberle, 2016). The simulation background and the state of natural convection in a porous medium made of two-dimensional square obstacles substantially impacted the mass transfer (Gasow et al., 2020). In addition, mass transport was a function of porosity and saturation (Ehlers & Häberle, 2016). On this occasion, it was theoretically explained using mathematical methods (Abdullah et al., 2011) and scaled porous analytics (Nelson & Bejan, 1998). For these reasons, the simulation and detection of liquid-gas phase change characterization are significant. Based on previous research, it was a potential solution in combining the efficiency of heating and cooling effectiveness. This research will be valuable for designing the blow mold cooling process on a factory scale to accommodate the situation. The specific objective of this work is to prove the cooling effectiveness and efficiency of heating numerically. It reconstructs the mold to reduce condensation while keeping the production cycle time. In this case, heating phenomena should apply the basic principle. The research result specified on

simulation of reference deliberated practical production expert naturally accommodated the heating and cooling process. Detection phenomena of the fluid movement in a scaled porous such as pressure, velocity, mass transfer rate, and heat flux are obligated.

The comparison of the research study can predict the solution to the manufacturing plastic contour issue. Calculation of cooling effectiveness to minimize the risk of condensation based on effective and efficient heat absorption on average using Equations 1 and 2 as follows:

$$q'' = \frac{2kg\beta L_r^2}{27\alpha\upsilon}(\Delta T)^2\left[1-\frac{9}{2Ra_H}\left(\frac{H}{L_r}\right)^4\right]^2 \quad (1)$$

$$q'' = 0.161\frac{k\Delta T}{H}\left(\frac{H}{L_r}\right)^{1/2} Ra_H^{1/4} \quad (2)$$

In manufacturing, both equations predict The *Rayleigh Number* (R_a) in the presence of gas layers in a cell that the heat penetrates to decrease its temperature before it is cooled excessively.

More heat penetrated the enclosure when the optical thickness of the gas layer closest to the heat source was lower than the second layer, resulting in higher cooling performance and lower rates of thermal failure (Nia et al., 2018).

There is a Governing Equation dealing with the cooling issue using porous. Simulation solves mathematic formulation of applied porous in cooling system reconstruction following in Equation 3.

$$\dot{E}_{in} + \dot{E}_g - \dot{E}_{out} = \dot{E} \quad (3)$$

Based on the literature arranged, the article places itself in the research about the cooling system of plastic molding. As information, it is typical that the cooling starts when the parison blows. In this situation, condensation appears. Besides, a heavy heat flow exists when parison sticks onto the mold interface. Based on the works of literature review, those are not allowed. The existing cooling method offered the maximum cooling rate; however, it has not considered the thermodynamic effect of cooling that could potentially control the heat rate with maintaining the cycle time. Simulation results detect the potential improvement of product quality by cells inside absorbing the heat and increasing thermal conductivity. In addition, heat changes water characteristics to increase The Nusselt Number. The paper follows the literature reviewed and adds some potential ways to become different. Its evidence is in simulation. The following steps were needed to generate this paper. Firstly, the experimental case-oriented. Secondly, adapted the character of observed behavior. This step needs evaluation and analysis of the cause and effect as research boundaries. Thirdly, simulated the original data, and fourthly, initiated the issue to calculate and retain the comparison. Finally, it proved the significant parameters for effective cooling and efficient heating.

2. Research Methodology

This research tries to resolve the plastic production problem by observing the manufacturing process, numerical analysis methods, literacy, and documenting. *Condensation* is an issue that has two option solutions which are reheating or cooling the air environment. The calculation properties are necessary, such as conditioning product temperature (T_h), backing plate cooler (T_c), depth of cooling, cooling area, cycle time, and critical point. After that, all properties are simulated and analyzed by using Ansys Fluent. There are three compulsory simulations: production process, optimum conditioning, and characteristics detection. Data are simulated and validated in this case to convince calculation results based on natural conditions. This method completes the research on the variance in the data processing (Kärger & Valiullin, 2013). Following (Pangaribawa & Fauzun, 2019), the simulation steps can be seen in Figure 1 as follows:

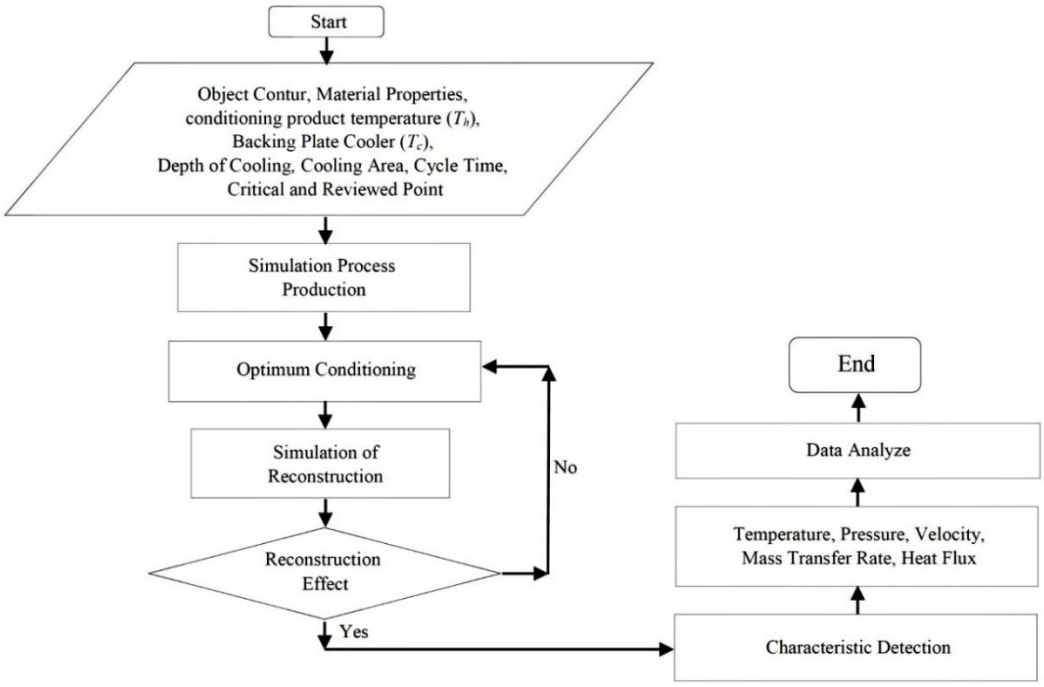

Figure 1. The simulation steps.

3. Results and Discussions

The simulation results in Tables 1 and 2 show data for cooling time versus the whole production time. The data provides time in seconds. Printed data following these steps: first, record parameters to hold valid simulation results; second, the information is literate as references. In addition, it considers errors simulation data up to 10%. Lastly, detect the fluid inner mold characteristics by the simulation. Briefly, the cooling time required the most considerable portion. The analysis result of samples 1 *l* and 250 *ml* indicated that the cooling time was 3/5 of the total production time. There were 15.5706 of 26.4206 sec and 15.641 of 26.491 sec, respectively. Seeking the comparison added respect to the research (Au & Yu, 2013).

Table 1. Comparison of cooling time to the whole production time of 1 *l*.

No.	Operation Names	Time (s)		
		Production Process (Reference)	Regular Simulation	Simulation of Reconstruction
1	Time of Blowing	15.15	15.6	15.5706
2	Total Cycle Time of 1 *l*	26	26.45	26.4206

Table 2. Comparison of cooling time to the whole production time of 250 *ml*.

No.	Operation Names	Time (s)		
		Production Process (Reference)	Regular Simulation	Simulation of Reconstruction
1	Time of Blowing	14.15	15.3	15.641
2	Total Cycle Time of 250 *ml*	25	26.15	26.491

Figures 2 and 3 show the direction of heat transfer during the cooling process. Color gradation shows the way heat transfers. The high temperature, which has upper-grade color, transfers to the right towards the smaller temperature. This point shows that $R_a \geq 10^5$ indicates more effectiveness than The Rayleigh Number $\geq 10^4$ in cooling. The potency is apparent in Figures 2-3 at the node measured, temperature, and time step.

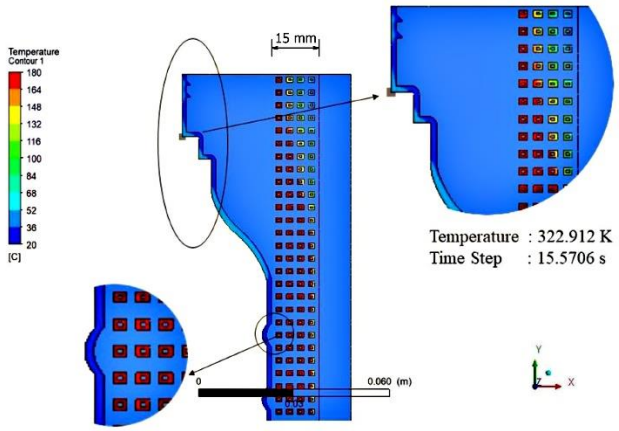

Figure 2. The direction of heat transfer during the cooling process of 1 *l*.

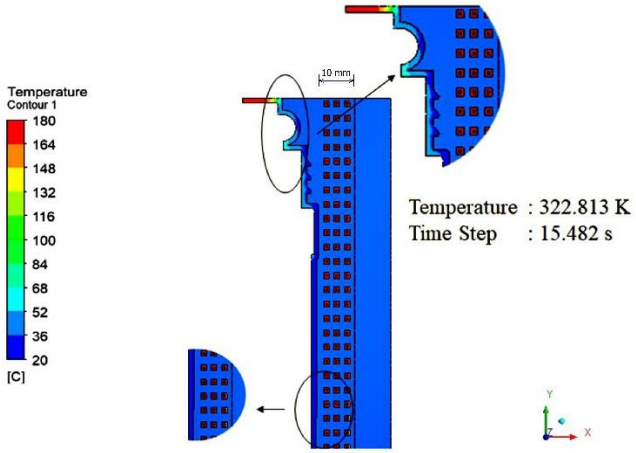

Figure 3. The direction of heat transfer during the cooling process of 250 *ml*.

Heat absorption and transfer through cells in the matrix show their different color levels. It indicates that the heat transferred from high temperature to lower temperature changed the other thermodynamics properties of the fluid.

Cell detection aims to get the value of fluid characteristics in the cell. The method simulates the natural state of a cooling process. The system observed should show cooling performance improvement, which was like has been researched by Pangaribawa & Fauzun (2019) using valid simulation results, numerically, and thermal failure rate reduction consideration (Industries, 2022) and (Belcher, 2017). In these situations, it is possible to show clearly the relation of cell geometry to the variation of The Rayleigh Numbers in the

cooling process of plastic packaging. Detections determine temperature, pressure, velocity, mass transfer rate, and heat flux parameters.

Figures 4 and 5 illustrate comparing plastic enclosures cooled in different Rayleigh Numbers. Figure 4 applies $R_a \geq 10^5$ while Figure 5 adjusts $R_a \geq 10^4$. The models have the same diameter, and their sizes are comparable. Figures 4-5 show the detailed potencies.

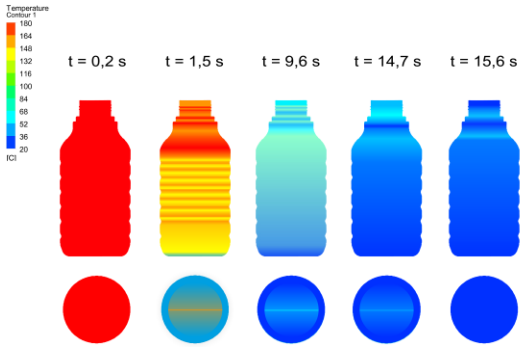

Figure 4. Contour plot of the cooling distribution of plastic packaging at $R_a \geq 10^5$, in different time steps.

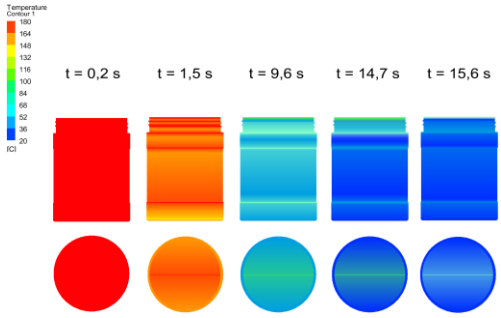

Figure 5. Contour plot of the cooling distribution of plastic packaging at $R_a \geq 10^4$, in different time steps.

Figure 4-5 show a contour plot of temperature distribution in different Rayleigh Number that indicates a minimum temperature of 20 ˚C and a maximum temperature of 180 ˚C. The phenomenon predicted that the R_a contributed to the rate of temperature decrease. It means that as long as 15.6 s, cooling of 1 *l* shows a significant order of the Rayleigh Number than 250 *ml*. Further to the effect of the Rayleigh Number discussed, the critical review of the Rayleigh Number in the depth of relative cooling is 15 mm, as shown in Table 3, while 10 mm is shown in Table 4.

Table 3. The Rayleigh Number at a relative depth of cooling 15 mm at a temperature of 23 °C.

Parameters	g	β	ΔT	H	α	v	Ra_H
Units	(m/s^2)	(K^{-1})	(K)	(m)	(m^2/s)	(m^2/s)	(-)
Values	9.8	0.000236	160	0.015	8.15E-06	9.37E-07	163314.8

Table 4. The Rayleigh Number at a relative depth of cooling 10 mm at a temperature of 23 °C.

Parameters	g	β	ΔT	H	α	v	Ra_H
Units	(m/s^2)	(K^{-1})	(K)	(m)	(m^2/s)	(m^2/s)	(-)
Values	9.8	0.000236	160	0.01	8.15E-06	9.37E-07	48389.58

Tables 3 and 4 show a relative extreme cooling distance (depth of cooling) of 15 mm, amount of The Rayleigh Number $\geq 10^5$, while at the space of 10 mm, the amount of The Rayleigh Number $\geq 10^4$. In other words, there are different Rayleigh Numbers.

Furthermore, the interface temperature can be used as a thermal failure rate reduction parameter because, as a prediction, gradient temperature reduction theoretically increases the thermal boundary layers, reducing condensation and increasing the crystalline rate on the polymer with stretching. In the rheology view, friction between solid materials is related to heating efficiency, as stated by (Vera-Sorroche et al., 2014), following the detection method by (Wen et al., 2012), detecting the interface temperature between the packaging and the mold during the production process indicates the increase of plastic heating that reveal in Tables 5 and 6. Both tables show the interface temperatures of 1 *l* and 250 *ml* packages; consecutively before and after mold reconstruction.

Table 5. Interface temperature detection of 1 *l* packaging.

Time (s)	Average temperature (°C)	
	Before Reconstruction	After Reconstruction
0.2	321	321
1.5	315	316
9.6	306	307
14.7	303	304
15.6	302	304
Average	310	311

Table 6. Interface temperature detection of 250 *ml* packaging.

Time (s)	Average temperature (°C)	
	Before reconstruction	After reconstruction
0.2	322	316
1.5	317	316
9.6	306	306
14.7	301	302
15.6	301	301
Average	309	308

Tables 5 and 6 show a difference in interface temperature between the conditions before and after the mold reconstruction. The 1 *l* packaging shows an apparent increase in temperature interfaces. The detection result follows the heating method to reduce condensate in the interface having a mold cooling system with $R_a \geq 10^5$. In contrast, at $R_a \geq 10^4$, the reconstruction does not show natural cooling control. The reconstruction of the cooling system, which is large and naturally controlled, is needed to prevent thermal shock and condensation refer to the research (Nia et al., 2018). The cell's function at $R_a \geq 10^4$ does not have much effect, as shown in Figures 2 and 3. It shows its saturate characteristics earlier, and the temperature level is at its highest grade. The probe pointed by arrows in Figures 2 and 3 indicates achievement of cooling due to the interaction of the cell with extreme cooling is the same as that of (Gauna & Zhao, 2017). In other

words, effective in cooling, there is also residual energy for heating efficiency research (Hsieh & Doan, 2018).

Reconstruction of the mold by applying cells to an actual process contributes to the cooling effectivity and heating efficiency. More precisely, the detection resulting from the cell numbers shows unorganized movement that brings potential effective heat transfer that is similar to the research of (Ehlers & Häberle, 2016), (Ould-Amer et al., 1998), and (Gasow et al., 2020). According to research, water as the cooler in cells states that water that had been heated and cooled to its original temperature had excess entropy (Tyrovolas, 2017). Random collisions were more likely to occur after recooling, causing the temperature to drop faster. Figures 6 and 7 show that fluid phase change into gas brings effective cooling by heat-absorbing. Research numerically for the effectivity of its cooling is following (Pangaribawa & Fauzun, 2019). As the research, the situation increases The Nusselt Number and heat rate transfer to enhance cooling (Li et al., 2012).

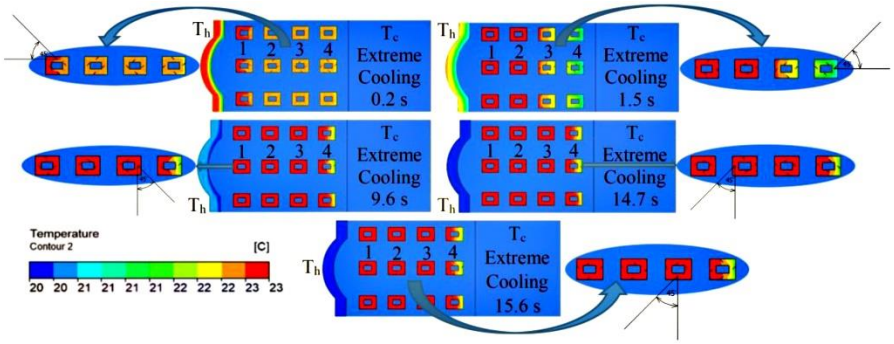

Figure 6. Contour plot of the cooling distribution of fluid in cells at $R_a \geq 10^5$, in different time steps.

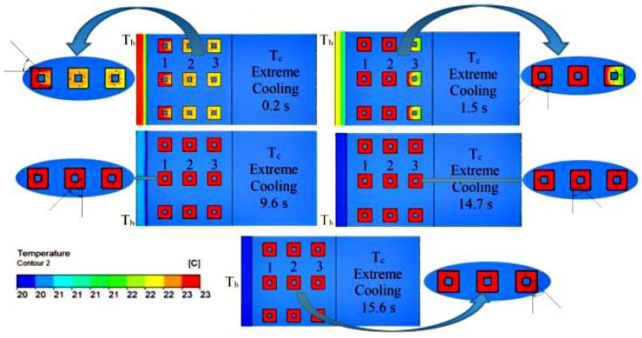

Figure 7. Contour plot of the cooling distribution of fluid in cells at $R_a \geq 10^4$, in different time steps.

Figures 6 and 7 give information on the cell location where detection of fluid characteristics as long as a cooling process. Heat transfer from the left side to the right side. There are four nodules for each of the cells. The changing of temperature represented by the color of the fluid in cells shows cells' capability to absorb the heat until it is saturated. The temperature change is red, indicating the water's saturated temperature. However, whether or not the phase will change depends on the pressure visible in Tables 7 and 8.

Table 7. Average of the velocity vector, pressure, and fluid phase with a degree of velocity resultant 45°, $R_a \geq 10^5$ using Fluent calculator function.

Parameters	Nodes	Coordinates			Average Velocity (u)	Average Velocity (v)	Average Pressure	Water Phase
		x	y	z				
Units		(m)	(m)	(m)	$(^m/_s)$	$(^m/_s)$	(MPa)	
Cells 1	1	-0.0233	-0.1017	0	-0.00028	0.000023	-3.3	Vaporization
	2	-0.0226	-0.1011	0	-0.00003	-0.000171	-3.3	Vaporization
	3	-0.0218	-0.1017	0	0.000194	0.000016	-3.3	Vaporization
	4	-0.0226	-0.1022	0	0.000040	0.000146	-3.3	Vaporization
Cells 2	5	-0.0199	-0.1017	0	-0.00020	0.000325	-3.3	Vaporization
	6	-0.0192	-0.1011	0	0.000117	0.000024	-3.3	Vaporization
	7	-0.0184	-0,1017	0	0.000194	-0.000056	-3.3	Vaporization
	8	-0.0192	-0.1022	0	-0.00011	-0.000099	-3.3	Vaporization
Cells 3	9	-0.0165	-0.1017	0	0.000089	-0.000151	-3.3	Vaporization
	10	-0.0158	-0.1011	0	0.000159	0.000042	-3.3	Vaporization
	11	-0.0150	-0.1017	0	-0.00006	-0.000161	-3.3	Vaporization
	12	-0.0158	-0.1022	0	0.000043	-0.000178	-3.3	Vaporization
Cells 4	13	-0.0131	-0.1017	0	-0.00002	0.000030	-3.3	Vaporization
	14	-0.0124	-0.1011	0	-0.00003	0.000179	-3.3	Vaporization
	15	-0.0116	-0.1017	0	-0.000004	-0.000008	-3.3	Vaporization
	16	-0.0124	-0.1022	0	0.000001	-0.000209	-3.3	Vaporization

Table 8. Average of the velocity vector, pressure, and fluid phase with a degree of velocity resultant 45°, $R_a \geq 10^4$ using Fluent calculator function.

Parameters	Nodes	Coordinates			Average Velocity (u)	Average Velocity (v)	Average Pressure	Water Phase
		x	y	z				
Units		(m)	(m)	(m)	$(^m/_s)$	$(^m/_s)$	(MPa)	
Cells 1	1	-0.0184	-0.0372	0	0.000026	-0.000002	-1.2	Vaporization
	2	-0.0178	-0.0367	0	-0.000007	0.000039	-1.2	Vaporization
	3	-0.0173	-0.0372	0	-0.000047	0.000011	-1.2	Vaporization
	4	-0.0178	-0.0377	0	-0.000007	-0.000027	-1.2	Vaporization
Cells 2	5	-0.0155	-0.0372	0	0.000058	-0.000020	-1.2	Vaporization
	6	-0.0150	-0.0367	0	0.000013	0.000024	-1.2	Vaporization
	7	-0.0144	-0.0372	0	-0.000056	-0.000021	-1.2	Vaporization
	8	-0.0150	-0.0377	0	-0.000011	-0.000007	-1.2	Vaporization
Cells 3	9	-0.0126	-0.0372	0	-0.000020	0.0000008	-1.2	Vaporization
	10	-0.0121	-0.0367	0	0.000029	0.000077	-1.2	Vaporization
	11	-0.0115	-0.0372	0	-0.000001	-0.0000165	-1.2	Vaporization
	12	-0.0121	-0.0377	0	0.000004	-0.0000051	-1.2	Vaporization

Table 7-8 adds the detailed information of Figures 6 and 7 that at a cell temperature of 23 °C, the pressure of -3.3 x 10^6 MPa, and $R_a \geq 10^5$. As a consequence, the fluid stage formed is a liquid-gas phase. So is at a pressure of -1.2 x 10^6 MPa and $R_a \geq 10^4$, determining the liquid-gas phase as mentioned in the properties water table (Cengel et al., 2019). The heating process causes molecular motion. Table 7-8 shows the directional irregularities of molecule velocity that indicate the characteristics of the liquid-gas phase. The fluid features in rectangular and square cells show in Tables 7-8, absorbing heat with a mass transfer rate through the control surface of 45°.

The concept of the cooling method is energy conservation. Calory should transform energy due to its inability to be destroyed. Heating the liquid to become a vapor is the natural phenomenon of cooling, and energy transfers into the cells and transforms the fluid into gas. Mathematical analysis of the technique are:

$$\dot{E}_{in} + \dot{E}_g - \dot{E}_{out} = \dot{E}$$

$$\left[-\bar{k}A\left(\frac{\partial T}{\partial x}+\frac{\partial T}{\partial y}+\frac{\partial T}{\partial z}\right)+\dot{m}c_{pf}T\right]+[q'''A]-\left[-\bar{k}A\left(\frac{\partial T}{\partial x}+\frac{\partial T}{\partial y}+\frac{\partial T}{\partial z}\right)-\bar{k}A\left(\frac{\partial^2 T}{\partial x^2}+\frac{\partial^2 T}{\partial y^2}+\frac{\partial^2 T}{\partial z^2}\right)+\dot{m}c_{pf}\left(T+\left(\frac{\partial T}{\partial x}+\frac{\partial T}{\partial y}+\frac{\partial T}{\partial z}\right)\right)\right]=A\overline{\rho c_p}\frac{\partial T}{\partial t}$$

There is no energy gain in the plastic cooling process, so

$$\left[-\bar{k}A\left(\frac{\partial T}{\partial x}+\frac{\partial T}{\partial y}+\frac{\partial T}{\partial z}\right)\right]-\left[-\bar{k}A\left(\frac{\partial T}{\partial x}+\frac{\partial T}{\partial y}+\frac{\partial T}{\partial z}\right)-\bar{k}A\left(\frac{\partial^2 T}{\partial x^2}+\frac{\partial^2 T}{\partial y^2}+\frac{\partial^2 T}{\partial z^2}\right)\right]=A\overline{\rho c_p}\frac{\partial T}{\partial t}-\dot{m}c_{pf}T+\dot{m}c_{pf}T+\dot{m}c_{pf}\left(\frac{\partial T}{\partial x}+\frac{\partial T}{\partial y}+\frac{\partial T}{\partial z}\right)$$

$$\left[-\bar{k}A\left(\frac{\partial T}{\partial x}+\frac{\partial T}{\partial y}+\frac{\partial T}{\partial z}\right)\right]+\bar{k}A\left(\frac{\partial T}{\partial x}+\frac{\partial T}{\partial y}+\frac{\partial T}{\partial z}\right)+\bar{k}A\left(\frac{\partial^2 T}{\partial x^2}+\frac{\partial^2 T}{\partial y^2}+\frac{\partial^2 T}{\partial z^2}\right)=A\overline{\rho c_p}\frac{\partial T}{\partial t}-\dot{m}c_{pf}T+\dot{m}c_{pf}T+\dot{m}c_{pf}\left(\frac{\partial T}{\partial x}+\frac{\partial T}{\partial y}+\frac{\partial T}{\partial z}\right)$$

$$\bar{k}A\left(\frac{\partial^2 T}{\partial x^2}+\frac{\partial^2 T}{\partial y^2}+\frac{\partial^2 T}{\partial z^2}\right)=A\overline{\rho c_p}\frac{\partial T}{\partial t}-\dot{m}c_{pf}T+\dot{m}c_{pf}T+\dot{m}c_{pf}\left(\frac{\partial T}{\partial x}+\frac{\partial T}{\partial y}+\frac{\partial T}{\partial z}\right)$$

$$\bar{k}A\left(\frac{\partial^2 T}{\partial x^2}+\frac{\partial^2 T}{\partial y^2}+\frac{\partial^2 T}{\partial z^2}\right)=A\overline{\rho c_p}\frac{\partial T}{\partial t}+\dot{m}c_{pf}\left(\frac{\partial T}{\partial x}+\frac{\partial T}{\partial y}+\frac{\partial T}{\partial z}\right)$$

$$\left(\frac{\partial^2 T}{\partial x^2}+\frac{\partial^2 T}{\partial y^2}+\frac{\partial^2 T}{\partial z^2}\right)=\frac{\overline{\rho c_p}}{\bar{k}}\frac{\partial T}{\partial t}+\frac{\dot{m}c_{pf}}{\bar{k}A}\left(\frac{\partial T}{\partial x}+\frac{\partial T}{\partial y}+\frac{\partial T}{\partial z}\right)$$

$$\left(\frac{\partial^2 T}{\partial x^2}+\frac{\partial^2 T}{\partial y^2}+\frac{\partial^2 T}{\partial z^2}\right)-\frac{\dot{m}c_{pf}}{\bar{k}A}\left(\frac{\partial T}{\partial x}+\frac{\partial T}{\partial y}+\frac{\partial T}{\partial z}\right)=\left[\frac{\overline{\rho c_p}}{\bar{k}}\frac{\partial T}{\partial t}\right].$$

Due to the detection of vaporization, so the equation should become

$$\left(\frac{\partial^2 T}{\partial x^2}+\frac{\partial^2 T}{\partial y^2}+\frac{\partial^2 T}{\partial z^2}\right)-\frac{\dot{m}L}{\bar{k}A}\left(\frac{\partial T}{\partial x}+\frac{\partial T}{\partial y}+\frac{\partial T}{\partial z}\right)=\left[\frac{\overline{\rho c_p}}{\bar{k}}\frac{\partial T}{\partial t}\right]$$

The fluid phase in the cell and increasing fluid mass transfer rate break down in Table 7-8 at the nodes in Figures 6-7. Also, the cell detection results indicate mass transfer rate, volume, and heat flux during the production time range in Table 9-10. In the tables, the simulation shows that the mass movement influenced the increasing or decreasing of the heat flux. The greater the mass move indicated, the more intense the heat transfer. The research shows that a more significant pore diameter resulted in a faster mass transfer rate (Li et al., 2012). It means that the fluid mass that moves is proportional to the energy absorbed per unit area and the unit of time. The liquid mass displaced indicates a convection process, such as the study (Abdullah et al., 2011). Meanwhile, Table 9 shows the cooling properties of plastic packaging, such as heat flux, volume, and mass transfer at The Rayleigh Number, $R_a \geq 10^5$. Besides that, Table 10 gives information about heat flux, volume, and mass transfer in $R_a \geq 10^4$.

Table 9. Heat flux, volume and mass transfer of cooling with $R_a \geq 10^5$ as long as 15.6 s.

Parameters	Nodes	Average Heat Flux	Average Volume	Average Mass Transfer
Units		$(^{Watt}/_{m^2})$	(mm^3)	(kg)
Cells 1	1	89344.7	80.212	0.00124
	2	102974.1	92.448	0.00143
	3	93215.1	83.686	0.00130
	4	85629.2	76.876	0.00119
Average		92790.8	83.305	0.00129
Cells 2	1	193659.6	173.863	0.00270
	2	138446.4	124.294	0.00193
	3	98430.2	88.368	0.00137
	4	103882.5	93.263	0.00145
Average		133604.7	119.947	0.00186
Cells 3	1	160714.4	144.286	0.00224
	2	180339.4	161.905	0.00252
	3	252565.6	226.748	0.00353
	4	135290	121.460	0.00189
Average		182227.3	163.600	0.00254
Cells 4	1	81499.2	73.168	0.00113
	2	108791.4	97.670	0.00152
	3	84459.3	75.826	0.00118
	4	81826.7	73.462	0.00114
Average		89144.2	80.031	0.00124

Table 10. Heat flux, volume and mass transfer of cooling with $R_a \geq 10^4$ as long as 15.6 s.

Parameters	Nodes	Average Heat Flux	Average Volume	Average Mass Transfer
Units		$(^{Watt}/_{m^2})$	(mm^3)	(kg)
Cells 1	1	26282.5	23.128	0.000360
	2	31110.4	27.377	0.000426
	3	25585.1	22.514	0.000350
	4	29404.3	25.875	0.000402
Average		28095.6	24.723	0.000384
Cells 2	1	24683.8	21.721	0.000338
	2	31773.7	27.960	0.000435
	3	23652.8	20.814	0.000324
	4	29561.2	26.013	0.000405
Average		27417.9	24.127	0.000375
Cells 3	1	25765.2	22.673	0.000353
	2	36059.4	31.732	0.000494
	3	26686.7	23.484	0.000365
	4	27617.3	24.303	0.000378
Average		29032.2	25.548	0.000397

It is evident in Table 9 that the average heat flux value at $R_a \geq 10^5$ is more significant than that shown in Table 10 at $R_a \geq 10^4$. At $R_a \geq 10^5$, this cooling process has a dome-shaped trend, as reported by (Nelson & Bejan, 1998). To clarify the trend, refer to Figure 8, which shows heat flux change in an increasing number of cells at $R_a \geq 10^5$ and $R_a \geq 10^4$ at 15.6 sec of manufacturing. Figure 8 shows that at $R_a \geq 10^4$, there is an insignificant heat flux increase than a cell before, or nearly flat. The detection results show that the optimum energy absorbed in the third cell is 29032.2 W/m^2. Decrease of heat flux by 5.56% (1614.3 W/m^2) than its cell before. In contrast, at $R_a \geq 10^5$, the peak was detected 182227.3983 W/m^2, creating a difference from before by 26.68% (48622.6933 W/m^2). The situation is unlike the cell reconstruction at $R_a \geq 10^4$. Although, it is close to the dome trends with a peak reached.

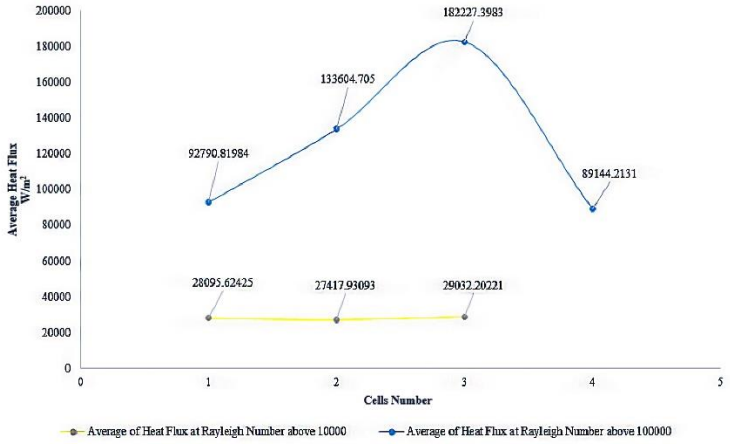

Figure 8. Correlation of heat flux characteristics and the cell number.

Figure 8 shows the correlation between heat flux characteristics and the cell number. Its heat flux represents cooling effectivity in various cells' positions and sizes. It is illustrated that cooling ability should correlate with the gap reconstruction. Figure 9 plots the simulation results. Figure 9 plots simulation results, a correlation of effectivity of cooling and heat flux at $R_a \geq 10^5$.

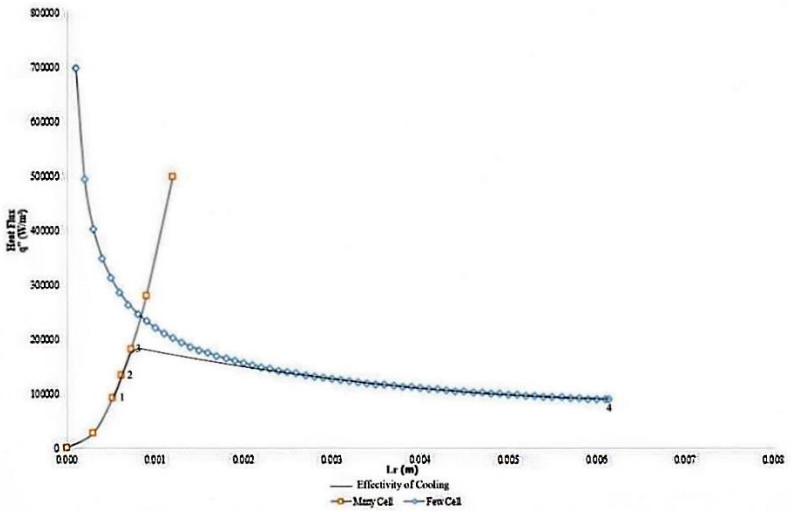

Figure 9. Correlation of effectivity of cooling and heat flux at $R_a \geq 10^5$.

Heat absorption occurred as long as 15.6 sec at $R_a \geq 10^5$ in the cell with a peak value. The cell cooling system does not cool the plastic packaging suddenly. Fluid in storage keeps the heat before the mold becomes cool while continuing the opening mold for subsequent cooling in time of stand ascent and time cutting of parison. Besides maintaining the interface temperature, this cooling characteristic anticipates findings in the plastic manufacturing process to prevent product defects due to excessive cooling (Brdlík, 2017).

The following graph describes the cooling performance characteristics with cells at $R_a \geq 10^4$. Figure 10 shows that the heat flux diagram at $R_a \geq 10^4$ does not reach its peak. The highest heat flux is in the third column cell of 29032.2 W/m^2, as shown in Figure 10 as follows:

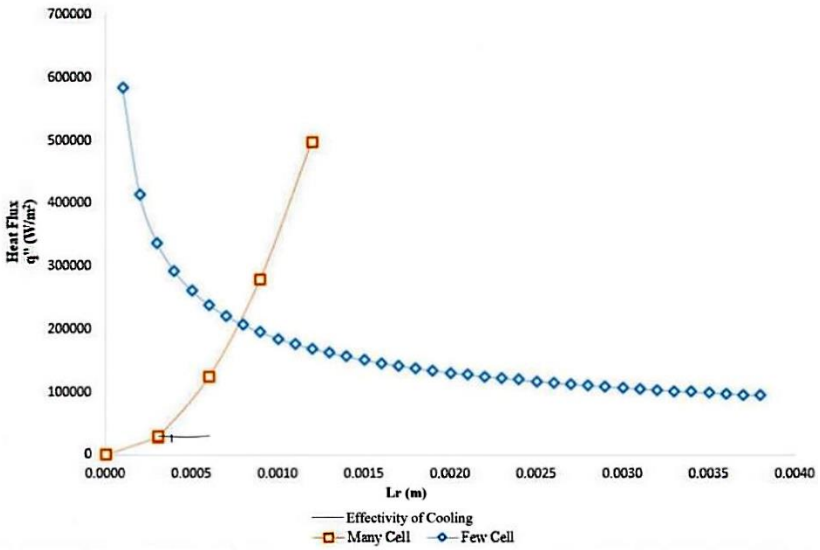

Figure 10. Correlation of effectivity of cooling and heat flux at $R_a \geq 10^4$.

As shown in Figure 10, the condition is not the same as in figure 9. There is no peak condition. It is predicted that the R_a did not influence too much.

In general, from a series of results and discussions, fluid inside the mold can potentially increase the thermal conductivity by process reconstruction of plastic mold. Based on the literature study, the heating process changed the fluid phase into gas and raised the Nusselt Number. Based on the simulation, it is revealed in a specific Rayleigh Number, $R_a \geq 10^5$. The effective cooling between the cooler and its heating part are not purely conduction; as an addition, porous involves moving particles.

4. Conclusions

A series of works have been carried out to achieve the specific objective of this work was to prove the cooling effectiveness and efficiency of heating numerically. Initial simulation results produced data for cooling time versus the whole production time. The analysis simulation result of samples 1 *l* plastic mold and 250 *ml* indicated that the cooling time was 3/5 of the total production time. There were 15.5706 of 26.4206 sec and 15.641 of 26.491 sec, respectively. Investigation of heat absorption and transfer through cells in the matrix indicates that the heat transferred from high temperature to lower temperature changed the other thermodynamics properties of the fluid. There also shows a contour plot of temperature distribution in different Rayleigh Numbers that indicates a minimum temperature of 20 ˚C and a maximum temperature of 180 ºC. The phenomenon predicted that the R_a contributed to the rate of temperature decrease revealed. Optimization of cooling distance shows a relative extreme cooling distance (depth of cooling) of 15 mm, amount of The Rayleigh Number $\geq 10^5$. In contrast, at the space of 10 mm, the amount of The Rayleigh Number $\geq 10^4$ is challenging. The difference in interface temperature between the conditions before and after the mold reconstruction is compared. In the 1 *l* packaging, there is an increase in temperature interface. Reconstruction of the mold by applying cells to an actual process contributes to the

cooling effectivity and heating efficiency. The comparison of the study research can predict the solution to the manufacturing plastic contour issue. It is calculating cooling effectiveness to minimize the risk of condensation based on effective and efficient heat absorption on average using available Equations. By simulation, a series of discussions of the result of research, the potential may apply in the plastic mold to reconstruct the space and its methods using filling-porous. It is relevant because the heating ability in the phase change of fluid that creates particular characteristics has the potential to make effective cooling.

Conflict of Interest

The authors confirm that there is no conflict of interest to declare for this publication.

Acknowledgments

Thank must go to the head of the department and faculty of engineering. The support of the grant numbers: 090/A.3-III/FT/III/2021 from Universitas Muhammadiyah Surakarta is fully acknowledged.

References

Abdullah, M.Z., Mujeebu, M.A., Gitano, H., Yaakob, Y., & Abdullah, M.K. (2011). Transient natural convection in a rectangular cavity filled with porous medium heated discretely at vertical wall. *Journal of Engineering Science*, *7*(1), 1-13. http://web.usm.my/jes/7_2011/JES-ART1-1-13.pdf

Au, K.M., & Yu, K.M. (2013). Conformal cooling channel design and CAE simulation for rapid blow mould. *International Journal of Advanced Manufacturing Technology*, *66*(1-4), 311-324. https://doi.org/10.1007/s00170-012-4326-6

Belcher, S.L. (2017). Blow Molding. In *Applied Plastics Engineering Handbook: Processing, Materials, and Applications: Second Edition* (Second ed.). Elsevier Inc. https://doi.org/10.1016/B978-0-323-39040-8.00013-4

Benrabah, Z., Mir, H., & Zhang, Y. (2013). Thermo-viscoelastic model for shrinkage and warpage prediction during cooling and solidification of automotive blow molded parts. *SAE International Journal of Materials and Manufacturing*, *6*(2), 349-364. https://doi.org/10.4271/2013-01-1397

Brdlík, P. (2017). The influence of cooling blow moulding process on mechanical behavior. *Journal of Interdisciplinary Research*, *461*, 119-120. https://www.oalib.com/paper/2329041#.Yitg9uhBy00

Cengel, Y.A., Boles, M.A., & Kanoğlu, M. (2019). Appendix 1 Property Tables and Charts. In *Thermodynamics an Engineering Approach* (Vol. 9, pp. 907-956). https://homepages.wmich.edu/~cho/ME432/Appendix1Udated_metric.pdf

Dale, W. (1984). Passive mold cooling and heating method. *19*. https://patents.google.com/patent/US4623497A/en

Davis, P.E.W. (1993). *United States Patent (19)*. https://patents.google.com/patent/US4515209A/en

Ehlers, W., & Häberle, K. (2016). Interfacial mass transfer during gas-liquid phase change in deformable porous media with heat transfer. *Transport in Porous Media*, *114*(2), 525-556. https://doi.org/10.1007/s11242-016-0674-2

Gasow, S., Lin, Z., Zhang, H.C., Kuznetsov, A.V., Avila, M., & Jin, Y. (2020). Effects of pore scale on the macroscopic properties of natural convection in porous media. *J. Fluid Mech.*, *891*, 891-912. https://doi.org/10.1017/jfm.2020.164

Gauna, E.A., & Zhao, Y. (2017). Numerical simulation of heat transfer in porous metals for cooling applications. *Metallurgical and Materials Transactions B: Process Metallurgy and Materials Processing Science*, *48*(4), 1925-1932. https://doi.org/10.1007/s11663-017-0981-1

Hsieh, Y.C., & Doan, M.H. (2018). Research on both the radiation heating and the cooling system inside the stretch blow molding machine CPSB-LSS12. *International Journal of Advanced Manufacturing Technology*, *98*(9-12), 2357-2364. https://doi.org/10.1007/s00170-018-2220-6

Industries, L. (2022). How to Solve Blow Molding Problems. In *Booklet* (pp. 1-11). LyondellBasell Industries. https://www.lyondellbasell.com/

Julianto, E., Siswanto, W.A., & Effendy, M. (2019). Characteristics of temperature changes and stress of float glass under heat radiation. *International Journal of Emerging Trends in Engineering Research*, *7*(9), 228-233. https://doi.org/10.30534/ijeter/2019/03792019

Kärger, J., & Valiullin, R. (2013). Mass transfer in mesoporous materials: The benefit of microscopic diffusion measurement. *Chemical Society Reviews*, *42*(9), 4172-4197. https://doi.org/10.1039/c3cs35326e

Kurtulus, K., Bolatturk, A., Coskun, A., & Gürel, B. (2021). An experimental investigation of the cooling and heating performance of a gravity die casting mold with conformal cooling channels. *Applied Thermal Engineering*, *194*(May). https://doi.org/10.1016/j.applthermaleng.2021.117105

Leonard, I., & Ryder, B. (1978). *United States Patent (19)*. https://patents.google.com/patent/US4091059A/en

Li, M., Wang, C., Liu, J., & Jing, Y. (2012). Pore size distribution effect on the mass transfer and reaction in a cylindrical porous gas sensitive medium. *Advanced Materials Research*, *550-553*, 2972-2976. https://doi.org/10.4028/www.scientific.net/AMR.550-553.2972

Nelson, R.A., & Bejan, A. (1998). *Constructal Optimization of Internal Flow Geometry in Convection*. *120*(2), 357-364. https://doi.org/10.1115/1.2824257

Nia, M.F., Nassab, S.A.G., & Ansari, A.B. (2018). Transient combined natural convection and radiation in a double space cavity with conducting walls. *International Journal of Thermal Sciences*, *128*(November 2017), 94-104. https://doi.org/10.1016/j.ijthermalsci.2018.01.021

Ould-Amer, Y., Chikh, S., Bouhadef, K., & Lauriat, G. (1998). Forced convection cooling enhancement by use of porous materials. *International Journal of Heat and Fluid Flow*, *19*(3), 251-258. https://doi.org/10.1016/S0142-727X(98)00004-6

Pangaribawa, M.R., & Fauzun. (2019). Numerical study of the mould contours effect on the plate cooling process heated from the side. *International Journal of Mechanical Engineering*, *6*(7), 14-20. https://doi.org/10.14445/23488360/ijme-v6i7p103

Suárez-Grau, F.J. (2021). Mathematical modeling of micropolar fluid flows through a thin porous medium. *Journal of Engineering Mathematics*, *126*(1), 1-25. https://doi.org/10.1007/s10665-020-10075-2

Tyrovolas, I.J. (2017). Explanation for the Mpemba effect. *Journal of Modern Physics*, *08*(12), 2013-2020. https://doi.org/10.4236/jmp.2017.812121

Vera-Sorroche, J., Kelly, A.L., Brown, E.C., Gough, T., Abeykoon, C., Coates, P.D., Deng, J., Li, K., Harkin-Jones, E., & Price, M. (2014). The effect of melt viscosity on thermal efficiency for single screw extrusion of HDPE. *Chemical Engineering Research and Design*, *92*(11), 2404-2412. https://doi.org/10.1016/j.cherd.2013.12.025

Wang, H., & Lei, C. (2020). A numerical investigation of conjugate thermal boundary layers in a differentially heated partitioned cavity filled with different fluids. *Physics of Fluids*, *32*(7). https://doi.org/10.1063/5.0013600

Wen, G.H., Tang, P., Yang, B., & Zhu, X.B. (2012). Simulation and characterization on heat transfer through mould slag film. *ISIJ International*, *52*(7), 1179-1185. https://doi.org/10.2355/isijinternational.52.1179